International Journal of Adhesion & Adhesives 31 (2011) 9–19

Contents lists available at ScienceDirect

International Journal of Adhesion & Adhesives

journal homepage: www.elsevier.com/locate/ijadhadh

Hygrothermal degradation of two rubber-toughened epoxy adhesives: Application of open-faced fracture tests

A. Ameli [a], M. Papini [b], J.K. Spelt [a,*]

[a] Department of Mechanical and Industrial Engineering, University of Toronto, 5 King's College Road, Toronto, Ontario, Canada M5S 3G8
[b] Department of Mechanical and Industrial Engineering, Ryerson University, 350 Victoria Street, Toronto, Ontario, Canada M5B 2K3

ARTICLE INFO

Article history:
Accepted 16 September 2010
Available online 23 October 2010

Keywords:
Hygrothermal
Absorption
Desorption
Degradation
Fracture toughness
Adhesive
Open-faced

ABSTRACT

The absorption/desorption properties of two commercial, toughened epoxy adhesive systems were evaluated gravimetrically, and by X-ray photoelectron spectroscopy (XPS) and dynamic mechanical thermal analysis (DMTA). Fracture tests on degraded open-faced DCB specimens showed that these two adhesive systems have very different degradation behaviors. The steady-state critical strain energy release rate, G_{cs}, of an adhesive system 1 decreased rapidly with an exposure time in various hot-wet environments, reaching a relatively low value that was stable for over one year, while that of adhesive system 2 remained unchanged for more than one and a half years. A degradation mechanism which accounts for the different characteristics of the two adhesive systems was proposed. A model of fracture toughness degradation, analogous to Fick's law, was then used to characterize the fracture toughness loss in an adhesive system 1, and the effects of temperature, RH and water concentration were evaluated. The results illustrate the wide variation in water absorption behaviors that can exist among toughened epoxy adhesives, and show how these differences relate to the degradation of fracture strength. The data were also used to assess the applicability of an exposure index (EI), defined as the integral of relative humidity over time, as a means of characterizing an aging history. The fracture strength degradation was measured after aging to achieve a range of EI values, and it was found that the strength loss was independent of the time–humidity path for sufficiently large EI.

© 2010 Elsevier Ltd. All rights reserved.

1. Introduction

It is known that hygrothermal degradation of adhesive joints is closely related to water absorption and desorption by the adhesive [1–5]. Toughened adhesives usually exhibit an anomalous absorption behavior, in which a simple Fickian model tends to overestimate the water concentration [6–8]. Dual Fickian models that superimpose two Fickian models, either acting in parallel [6,7,9], or sequentially [10], have been used successfully to characterize the anomalous water diffusion behavior. Unlike absorption, water desorption behavior is normally Fickian [11]. The existence of retained water after drying at temperatures below the glass transition temperature, T_g, has been reported in the literature [12–15]. Zhou and Lucas showed that the retained water after low-temperature desorption was related to the amount of water molecules that formed strong bonds with the epoxy constituents [13].

The absorbed water molecules in an epoxy can exist in either the free or bound states [3,4,16]. Free water molecules act as a plasticizer, strongly reducing T_g and the modulus of elasticity [17]. The water molecules that are tightly bound to the epoxy constituents can act as intermolecular joints causing an increase in the modulus of elasticity [18]. Such bound water is believed to also cause irreversible damage, such as chain scission, hydrolysis, crack initiation, crack growth, and subsequent loss of material [19]. In addition, water can disrupt the bonds at the interface between the adhesive layer and the adherends, causing irreversible damage in the interphase region [11].

Conventional closed joints are not well suited for degradation studies, because the degradation is not uniform and the water diffusion path is long, causing degradation experiments to be lengthy. Since the fracture results from testing such joints do not represent a discrete state of moisture degradation, it is impossible to apply the measured properties directly to other joint configurations or ageing environments [20]. Therefore, open-faced specimens have been utilized to achieve a spatially uniform state of degradation, as well as to accelerate the aging process by shortening the diffusion path of water into the adhesive layer [20–23].

This paper describes the absorption and desorption profiles of two different rubber-toughened epoxy adhesives. XPS and DMTA analyses were carried out to explain the differences in the gravimetric measurements. Open-faced double cantilever beam (DCB) specimens were then used to accelerate the water absorption and

* Corresponding author. Tel.: +1 416 978 5435; fax: +1 416 978 7753.
E-mail address: spelt@mie.utoronto.ca (J.K. Spelt).

0143-7496/$ - see front matter © 2010 Elsevier Ltd. All rights reserved.
doi:10.1016/j.ijadhadh.2010.10.001

desorption processes, and measure the resulting change in fracture strength. A degradation model analogous to Fick's law was proposed to characterize the loss of fracture strength in adhesive system 1, and the effects of changes in temperature, RH and water concentration on the model parameters were investigated. The relationship between the fracture strength and the exposure history was also evaluated (i.e. the effects of different combinations of water concentration and exposure time at a given temperature). A degradation mechanism was proposed which accounts for the different characteristics of the two adhesive systems.

2. Experimental procedure

The degradation of the fracture properties of two highly toughened, heat-cured structural epoxy adhesives (Table 1) was measured using open-faced double cantilever beam (DCB) specimens (Fig. 1). Adhesive 2 was used as the secondary adhesive layer in all the joints. Gravimetric measurements on cast, bulk adhesive wafers were used to characterize the water diffusion behavior. The recommended curing profile of at least 30 min at 180 °C was used for the primary and secondary bonds of the open-faced DCB fracture specimens, and the wafers used in the diffusion measurements. Cure was monitored using a thermocouple embedded in the adhesive layer.

Table 1
Mechanical and physical properties of adhesives 1 and 2 as supplied by the manufacturers.

Adhesive	Elastic modulus E, MPa	Poisson ratio, v	Tensile strength, σ_y, MPa	Cured density g/cm^3
Adhesive 1	1.96	0.45	44.8	1.50
Adhesive 2	1.73	0.39	N/A	1.14

2.1. Gravimetric measurements

Mass uptake measurements have been made under various combinations of temperature and RH on cast wafers of these same two adhesives in [10]. Table 2 shows the environmental conditions that were used in Ref. [10], the saturated salt solutions used to generate the atmospheres [20,24], and the amount of water vapor present per unit volume of gas [25]. After saturation, the wafers had been dried in a vacuum oven containing anhydrous calcium sulphate at 40 °C for up to 90 days. The absorption and desorption measurements have been repeated on three wafers at each exposure condition [10]. The temperature–humidity

Table 2
Exposure conditions for the gravimetric samples of Ref. [10] and the present open-faced specimens, together with the saturated salt solutions used and the ambient water concentration achieved at each condition.

RH (%)	Salt solution	Ambient water concentration (g/m^3)			
		T=20 °C	T=40 °C	T=50 °C	T=60 °C
43	K_2CO_3	7.4	21.7	35.2	55.1
82	KCl	14.1	41.5	67.1	105.1
95	K_2SO_4	16.3	48.0	77.8	121.7

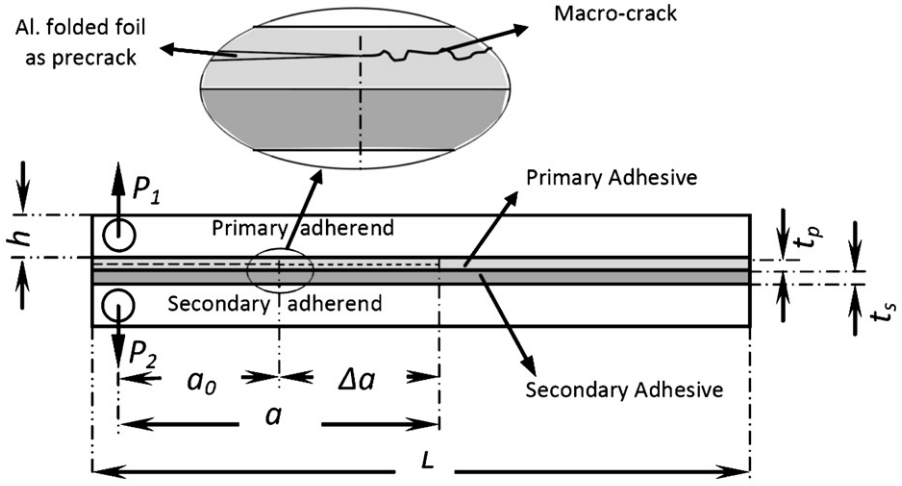

Symbol	Parameter	Size
L	Specimen length	~ 250 mm
h	Adherend thickness	12.7 mm
t_p	Primary bond thickness	0.4 mm
t_s	Secondary bond thickness	0.4 mm
w	Adherend width	19-21 mm
a_0	Starting length	~ 40 mm
Δa	Crack length increment	Variable
a	Crack length	Variable
P_1	Upper adherend load	Variable
P_2	Lower adherend load	Variable

Fig. 1. Configuration and dimensions of the open-faced DCB joints (not to scale).

conditions of Table 2 were also used for the aging of the present open-faced DCB specimens, as described below.

2.2. Dynamic mechanical thermal analysis

Cast wafers of adhesives 1 and 2 (approximately 10×20 mm^2 with 0.8 mm thickness) in the fresh, wet and dried states were tested in a dynamic mechanical thermal analyzer. The wafers were subjected to a frequency of 1 Hz, a tensile strain of 0.1% and a temperature ramp of 10 °C/min between 30 and 190 °C. The peak of the loss modulus versus temperature curve was used as an indicator of the glass transition temperature, T_g.

2.3. Open-faced DCB specimen fabrication

The DCB adherends were AA6061-T6 aluminum alloy pretreated using the P2 sulfuric acid etch method [26]. The primary adhesive layer of 0.4 mm thickness was cured onto the primary adherend using a backing plate coated with a polytetrafluroethylene release agent which had been baked dry (Fig. 1). After curing, the backing plate was removed and the open-faced specimens were degraded for varying times under the exposure conditions of Table 2. The XPS analysis showed that insignificant amounts of the release agent transferred to the free surface of the primary adhesive. The degraded specimens were then dried in a vacuum oven containing anhydrous calcium sulphate at 40 °C for approximately 7 days. The objective was to measure the irreversible effects of degradation by eliminating any reversible effects of water absorption, such as plasticization [21]. To increase the mechanical interlocking and ensure a strong bonding between the primary and secondary adhesive layers, the primary adhesive layer surface was roughened using 100 grit sandpaper, acetone wiped and dried before the secondary bonding. The roughening process removed less than 25 μm of the primary adhesive layer. To make a complete DCB joint, the open-faced specimen was then bonded to a second adherend using adhesive 2 and the same curing profile as for the primary bonding.

To investigate whether the second cure cycle had any effect on the fracture toughness of the primary layer of an adhesive, fracture tests were carried out on un-aged closed DCB joints made from a single layer of an adhesive 1. The difference between the average G_{cs} values for specimens that were cured once and twice was only 4%, which was statistically insignificant (t-test, 95% confidence). It was thus assumed that the primary layer was fully cured during the first cure and unaffected by the secondary bonding process. More details about the open-faced fabrication procedure can be found in [27].

The crack initiation geometry was created by embedding a folded 10 μm aluminum foil within the primary adhesive layer. To minimize the possibility of mechanical damage to the specimen edges after curing, the very small amount of residual adhesive that had flowed from the edges of the open-faced DCB specimens was removed, using a gentle wet sanding process (300 grit). To further improve the visibility of the crack, the bondline was finished by hand with 600 grit sandpaper. A very thin layer of white paper correction liquid, diluted with hexane, was then applied to the specimen edges to assist in the identification of the macro-crack tip.

2.4. Fracture test methodology

The mixed-mode fracture tests were conducted using a servo-electric load frame and the load jig of [28]. All tests were conducted at a loading phase angle $\psi = 27^\circ$, where $\psi = \arctan([G_{IIc}/G_{Ic}]^{0.5})$, and G_{Ic} and G_{IIc} are the modes I and II components of the strain energy release rate. The specimen was loaded in discrete small steps, while viewing the crack tip (the tip of the furthest advanced micro-crack) through a microscope to detect the onset of crack propagation at the critical load. The crack length, a (Fig. 1), was determined to an accuracy of ± 20 μm, using an optical microscope on a micrometer stage having a field of view of 2 mm. A discussion of the discrete loading method methodology and its validity can be found in [29]. A beam-on-elastic-foundation model was used to calculate the steady-state critical strain energy release rate, G_{cs} [30].

3. Results and discussion

3.1. Water absorption and desorption

Sequential dual Fickian (SDF) and simple Fickian models (Appendix) were used to characterize the water absorption and desorption behaviors, respectively, in both adhesives. A nonlinear, least-squares optimization approach was used in MATLAB® programming to find the best-fit of the SDF model to the experimental data points [10]. Fig. 2 shows the gravimetrically measured fractional mass uptake, M_t versus the square root of time ($t^{1/2}$), and the best fits based on the SDF model at 60 °C-95% RH and 60 °C-82% RH for adhesives 1 and 2. M_t is defined as the total mass uptake of water at time t expressed as a percentage of the initial mass of the adhesive. After the initial linear Fickian diffusion and the onset of a plateau, a second mass increase was observed for both adhesives in most of the exposure conditions. Hence, a simple Fickian model would overestimate the experimental results, especially at high T and RH, and at intermediate times. This anomalous behavior was captured by the SDF model [10]. Fig. 2 also depicts the fractional mass loss during drying versus $t^{1/2}$ and the least-squares fits based on a simple Fickian model for both adhesives. The mass of the samples decreased with drying time according to Fick's law and reached a constant minimum value of fractional retained water, M_r (mass of retained water expressed as a percentage of the initial mass of the adhesive). The required SDF absorption parameters (D_1, D_2, $M_{1\infty}$, $M_{2\infty}$, t_d) and the simple Fickian desorption parameters (D_d, M_r) for both adhesives are given in Appendix.

In general, adhesive 2 was more resistant to water absorption than adhesive 1, and so all the SDF parameters for adhesive 2 were less than those for adhesive 1 at the same exposure condition. The main difference between the desorption behavior of adhesives 1 and 2 was the minimum fractional retained water after drying, M_r (Table 6 in Appendix). For adhesive 1, M_r increased proportionally with the increase of temperature, RH, M_∞ (sum of $M_{1\infty}$ and $M_{2\infty}$) and the

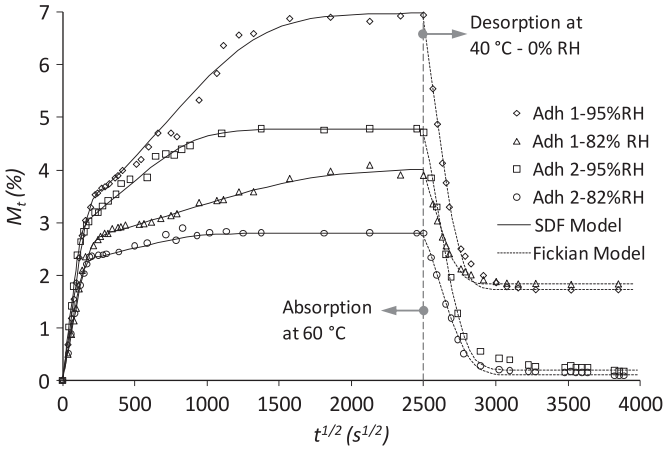

Fig. 2. Gravimetrically measured fractional mass uptake and loss versus square root of time. The least-squares fits based on the SDF model for mass uptake, and the simple Fickian model for drying are shown for both adhesives 1 and 2. Each data point is the average of the results for three cast wafers.

ambient water concentration [10]. M_r/M_∞, which represents the ratio between the bound and total water molecules (see Section 3.3), was negligible (approximately 3%) for adhesive 2 while it was much greater for adhesive 1, varying between 24% and 60% depending on the exposure condition. A higher temperature and lower RH resulted in higher values of M_r/M_∞, and hence higher ratios of bound to free water molecules.

3.2. XPS analysis

The significant difference in the amount of retained water in adhesives 1 and 2 after drying was investigated using XPS on samples in three conditions: fresh (as-cured), saturated wet and dried after saturation. The wet samples of adhesives 1 and 2 were saturated at 60 °C-95% RH giving M_∞ of 6.98% and 4.78%, respectively. The dry samples were made by drying saturated wet samples at 40 °C in a vacuum oven containing anhydrous calcium sulphate for one week. Three repetitions were carried out at each condition. Analysis areas had a diameter of 500 μm. Elemental compositions were determined from peak areas. Table 3 shows the O/C ratios for the two adhesives in the fresh, saturated wet and dried conditions. As expected, the ratios were largest in the wet condition, since the samples included free water molecules, and the values were proportional to M_∞, being greater for adhesive 1 than for adhesive 2. Furthermore, the O/C ratio increased from the fresh state to the dried state after an initial saturation. This increase was related to the chemical interactions between the adhesives constituents and water molecules such as hydrolysis, as has been explained by Xiao et al. [31]. In the dried condition, the O/C ratio of adhesive 1 was greater than that of adhesive 2, which agrees qualitatively with the greater amount of retained water in adhesive 1.

Table 3
Elemental composition ratio of O/C for the fresh, saturated wet and dried conditions for adhesives 1 and 2.

Condition	O/C ratio in percentage	
	Adhesive 1	Adhesive 2
Fresh	13.5	13.2
Saturated wet	22.6	20.1
Dried	18.3	16.4

Fig. 3 shows the O1s peaks associated with various chemical bonds (binding energies) for fresh, saturated wet and dried samples of adhesives 1 and 2. The O1s peak at approximately 533 eV was dominant in all cases and corresponded to the one observed in a cured di-glycidyl ether of bisphenol A (DGEBA) bulk epoxy sample, as reported in [32]. O1sA at 534 eV was also detected in each case, and was thus related to adhesive constituents. It is hypothesized that the third peak, O1sB at 531.5 of eV, was related to a bond associated with water molecules, since it was present in the wet samples of both adhesives, but not in the fresh and dried samples of adhesive 2, nor was it significant in the fresh adhesive 1. The significant amount of O1sB present in the dried samples of adhesive 1 qualitatively supports the gravimetric results indicating that a considerable amount of absorbed water in adhesive 1 could not be removed during the drying process. The O1sB peak was not detected in the dried adhesive 2 samples, which was consistent with the negligible amount of retained water in adhesive 2.

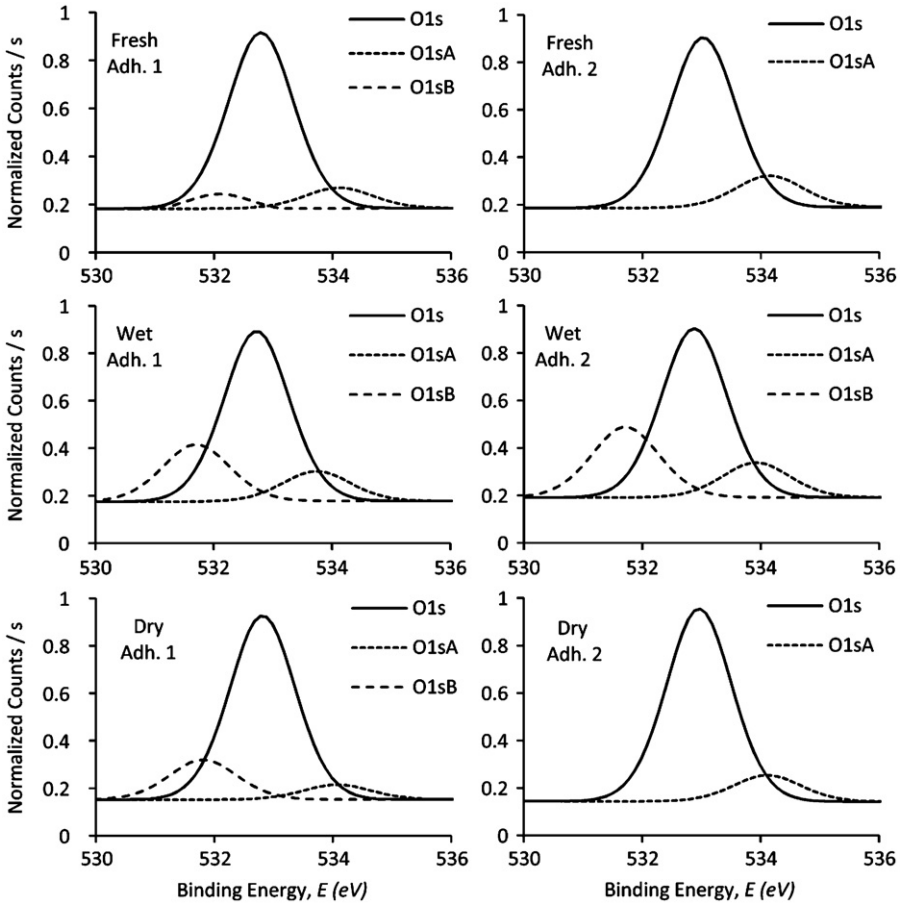

Fig. 3. An XPS 1 s oxygen peaks (O1s, O1sA and O1sB) for fresh, saturated wet and dried samples of adhesives 1 and 2.

Furthermore, The XPS analysis of the fracture surfaces of aged and dried open-faced DCB joints (three replications) indicated the presence of an O1sB in the fracture surface of joints, in which adhesive 1 was the primary layer, but not in those in which adhesive 2 was the primary layer. This was expected since the open-faced joints had been aged and dried before the fracture tests, and so their XPS spectra resembled those of dried wafers. Indeed, the ratio of the O1sB peak height to that of the total O1s obtained from adhesive 1 open-faced joints (O1sB/O1s = 13%) was comparable to that in the dried wafer sample of adhesive 1 (O1sB/O1s = 10%).

3.3. Dynamic mechanical thermal analysis

Figs. 4 and 5 show representative examples of the loss modulus, E' as a function of temperature, T, for samples of adhesives 1 and 2, respectively, in the fresh, wet and dried conditions, as measured using the DMTA. Table 4 summarizes the conditioning history and the T_g values measured from the E'–T curves for both adhesives. In the wet samples of both adhesives, the peak of the E' versus T curves shifted to the left indicating a significant drop in T_g. Also, at elevated temperatures, the loss modulus of the wet samples became lower than that of the fresh adhesive as observed in [33,34]. The rate of T_g decrease for adhesives 1 and 2 was approximately 9 and 7 °C, respectively, per 1% increase in the water concentration. This is in good agreement with the value of 8 °C per 1% reported for DGEBA epoxy resins [35]. As seen in Table 4, the plasticizing effect was reversible with drying causing T_g to return to the value of the fresh samples in both adhesives, irrespective of the amount of retained water. Noting that the decrease in T_g with absorbed water is attributed to the plasticization effect of free water molecules, it can be concluded that the retained water molecules in adhesive 1 were not free and were strongly bound to the adhesive constituents, since T_g was unaffected by the presence of the retained water in adhesive 1.

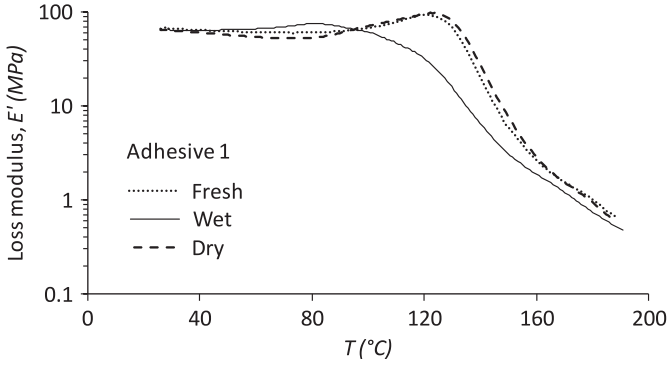

Fig. 4. The variation of loss modulus versus temperature for fresh (Table 4: sample Fresh A1), wet (Table 4: sample Wet B1) and dried (Table 4: sample Dry B1) samples of adhesive 1.

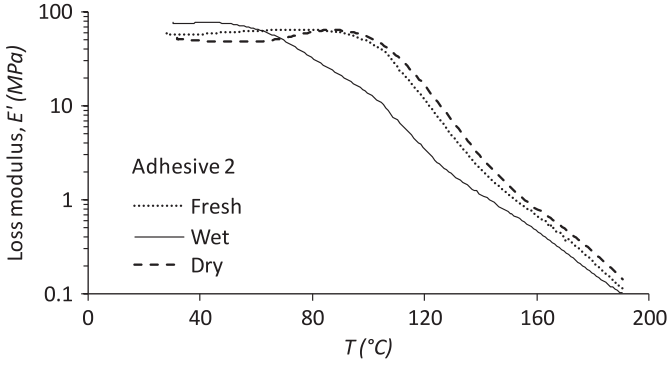

Fig. 5. The variation of loss modulus versus temperature for fresh (Table 4: sample Fresh A2), wet (Table 4: sample Wet A2) and dried (Table 4: sample Dry A2) samples of adhesive 2.

Table 4
The conditioning history and the fractional mass uptake, M_t reached before DMTA testing and T_g for different samples of adhesives 1 and 2. The drying condition for the saturated samples was 14 days at 40 °C.

Sample		Conditioning	M_t (%)	T_g (°C)
Adhesive 1				
Fresh	A1	Cured and dried	0.00	121
Wet	A1	Saturated at 60 °C-43% RH	1.62	111
Wet	B1	5 Days aging at 60 °C95% RH	4.54	75
Wet	C1	7 Days aging at 60 °C-95% RH	4.81	81
Dry	A1	Saturated at 40 °C-43% RH and dried	0.86	124
Dry	B1	Saturated at 60 °C-43% RH and dried	0.98	122
Dry	C1	Saturated at 60 °C-95% RH and dried	1.76	121
Adhesive 2				
Fresh	A2	Cured and dried	0.00	75
Wet	A2	Saturated at 60 °C-95% RH	4.78	42
Dry	A2	Saturated at 60 °C-95% RH and dried	0.16	78

To support this conclusion further, the DMTA temperature scan test was repeated on some of the wet and dried samples of adhesive 1. As expected, because of the high temperatures reached in the DMTA (up to 190 °C), the gravimetric measurements taken after the first scan showed some mass loss in both wet and dry samples, as also reported in [13,19]. This mass loss during the first scan in the wet samples caused T_g to increase from 75 °C in the first scan to 111 °C in the second scan. There was a negligible change in T_g of the dried samples (112 °C in the first scan and 113 °C in the second scan), in spite of the decrease in the retained water during the first scan (1.68% and 1.26% before and after the first scan). Therefore, the retained water after drying had no plasticizing effect, supporting the conclusion that the retained water molecules were tightly bound to the adhesive constituents.

3.4. Fracture strength degradation

3.4.1. G_{cs} of fresh joints

The fracture strength of the primary layer in undegraded open-faced specimens was difficult to measure, because of the tendency of the crack to kink towards and propagates in the secondary layer even though it initiated at the foil embedded in the primary layer. This problem did not occur when the primary layer was aged, since the reduced fracture toughness of the degraded primary layer compared to that of the fresh secondary layer resulted in crack path that remained in the primary layer. Therefore, the G_{cs} of the un-aged (fresh) open-faced DCB specimens was estimated, using a standard closed DCB (single adhesive layer). It is known that the fracture toughness of adhesive joints is significantly affected by the bondline thickness in single-layered specimens [30,36–38]. Therefore, in order to establish the G_{cs} corresponding to a fresh open-faced specimen, using a standard DCB with a single adhesive layer, it was necessary to determine whether to make the single layer equal to the primary adhesive thickness or the sum of the primary and secondary layers. Experiments were conducted with different combinations of primary and secondary adhesive thicknesses, and it was concluded that the thickness of the layer in which the crack propagated (primary or secondary) was the parameter affecting the fracture strength of the joint, not the total thickness of the primary and secondary layers. In other words, the

crack propagated in one adhesive layer as if the other layer did not exist. Therefore, the G_{cs} of a single-layered DCB specimen, with a bondline thickness, equal to that of the primary layer in open-faced DCB specimens, was used as the reference fracture toughness in the evaluation of the amount of degradation for aged open-faced DCB specimens. At a phase angle of 27° and a bondline thickness of 400 μm, these reference values were 4160 Jm^{-2} (six replications with standard deviation of 260 Jm^{-2}) and 4380 Jm^{-2} (six replications with standard deviation of 284 Jm^{-2}) for adhesive systems 1 and 2, respectively.

3.4.2. G_{cs} degradation in adhesive system 1

The fracture strength of the degraded open-faced DCB specimens of adhesive system 1, measured as the steady-state critical strain energy release rate, $G_{cs}(t)$, was a strong function of the exposure time in the early stages of degradation. The amount of degradation was quantified by $\Delta G_{cs}(t)$; the decrease in G_{cs}

$$\Delta G_{cs}(t) = G_{cs}(0) - G_{cs}(t). \quad (1)$$

where $G_{cs}(0)$ is the reference fracture strength of the undegraded specimens. Figs. 6 and 7 show the variation of $\Delta G_{cs}(t)$ with the square root of an exposure time (up to approximately 400 days) for adhesive system 1 at three different RH and temperatures of 60 and 40 °C, respectively. Fig. 8 shows similar results for temperatures of 20 °C (at 95% RH) and 50 °C (at 95% RH and 82% RH) up to approximately 600 days. It is seen that the fracture strength decreased even at very short exposure times and at all water concentrations, even those that were very low. $\Delta G_{cs}(t)$ then reached a plateau value (ΔG_{cs}^{∞}). It was hypothesized that the variation of $\Delta G_{cs}(t)$ with time could be modeled, using a simple Fickian-type relation since it appeared to depend mostly on the amount of water absorbed. Therefore,

$$\Delta G_{cs}(t) = \left[1 - \frac{8}{\pi^2}\sum_{n=0}^{\infty}\frac{1}{(2n+1)^2}\exp(-D_{\deg}t)\right]\Delta G_{cs}^{\infty} \quad (2)$$

where $D_{\deg}$ (day^{-1}) is defined as a degradation coefficient, which reflects the rate of degradation. Figs. 6–8 show the nonlinear least-squares fits of Eq. (2) to the experimental $\Delta G_{cs}(t) - t^{1/2}$ data. Overall, the agreement was reasonable, although Eq. (2) overestimated the degradation by approximately 10% near the end of the rising portion of curves at higher RH. Although, this indicates that a dual Fickian-type model would result in a better representation of the fracture strength loss, similar to the dual stage Fickian behavior observed with water diffusion, a simple Fickian-type relation was assumed in this case because of the limited number of experimental data points available. One of the advantages of modeling the strength loss with Eq. (2) was that the influence of T and RH on the degradation behavior could be evaluated conveniently by assessing their effects on ΔG_{cs}^{∞} and the degradation coefficient ($D_{\deg}$).

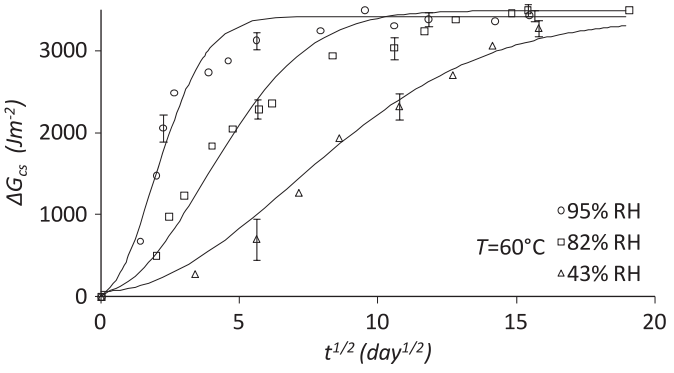

Fig. 6. Measured loss of G_{cs} versus square root of exposure time and the least-squares Fickian-type fits at 60 °C and three different RH. Adhesive system 1 tested at a phase angle of 27°. Each data point without an error bar is an average of at least 20 individual crack growth measurements within one DCB specimen. Each data point with an error bar (± standard deviation) is an average value obtained from three different DCB specimens (at least 20 individual crack growth measurements from each).

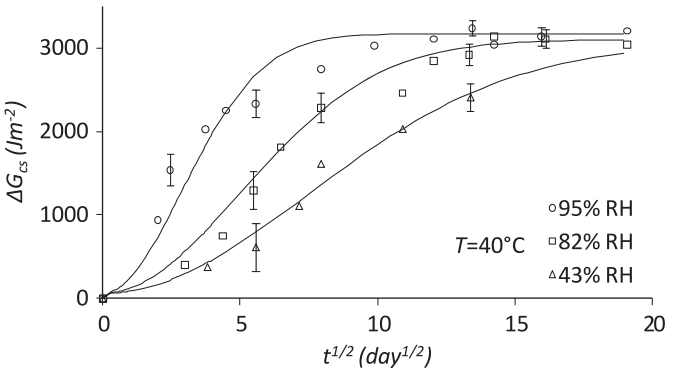

Fig. 7. Measured loss of G_{cs} versus square root of exposure time and the least-squares Fickian-type fits at 40 °C and three different RH. Adhesive system 1 tested at a phase angle of 27°. Each single data point is an average of at least 20 crack growth measurements within one DCB specimen. Each data point with an error bar (± standard deviation) is an average value obtained from three different DCB specimens (at least 20 individual crack growth measurements from each).

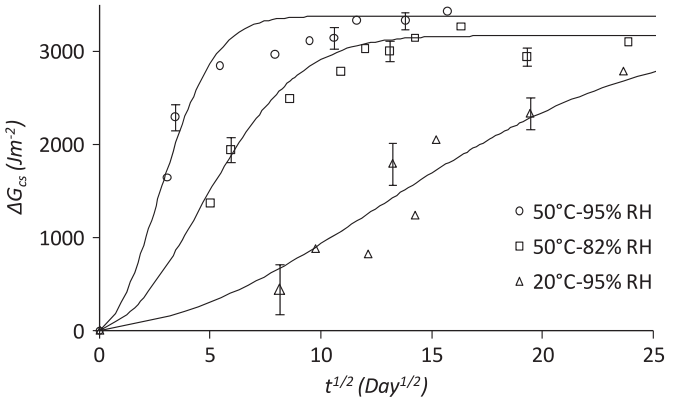

Fig. 8. Measured loss of G_{cs} versus square root of exposure time and the least-squares Fickian-type fits at 20 and 50 °C. Adhesive system 1 tested at a phase angle of 27°. Each single data point is an average of at least 20 crack growth measurements within one DCB specimen. Each data point with an error bar (± standard deviation) is an average value obtained from three different DCB specimens (at least 20 individual crack growth measurements from each).

Table 5
Maximum G_{cs} decrease (ΔG_{cs}^{∞}) obtained by curve fitting at different T and RH combinations.

RH (%)	ΔG_{cs}^{∞} (Jm^{-2})			
	T=20 °C	T=40 °C	T=50 °C	T=60 °C
43	–	3220	–	3280
82	–	3150	3160	3450
95	3180	2990	3380	3420
Average	3180	3120	3270	3380
Standard deviation	–	117	–	89

Table 5 shows the maximum decrease in G_{cs} (ΔG_{cs}^{∞}) obtained by a nonlinear curve fitting the data at different combinations of T and RH (Figs. 6–8). It is seen that the dependence of ΔG_{cs}^{∞} on RH was very weak at a given T. Moreover ΔG_{cs}^{∞} did not appear to follow a trend with temperature, and the maximum difference between the ΔG_{cs}^{∞} values obtained at different temperatures was in the experimental

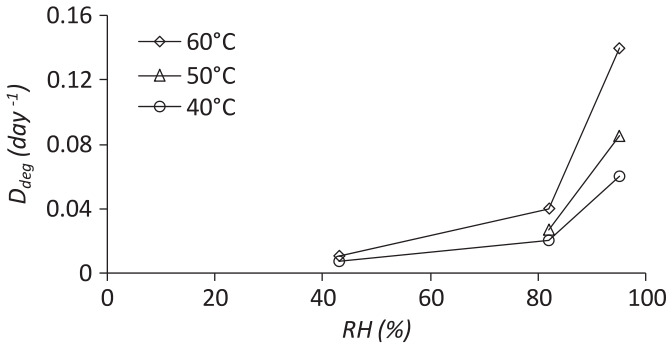

Fig. 9. Variation of the degradation coefficient of adhesive system 1 with RH at 60 and 40 °C. The lines are to guide the eye.

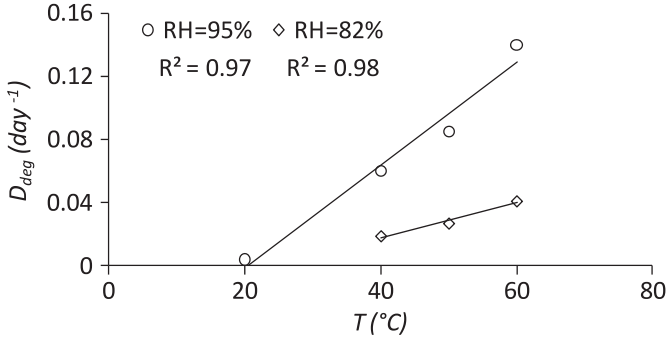

Fig. 10. Variation of the degradation coefficient of adhesive system 1 with temperature at 95% and 82% RH. The lines show the least-squares fits.

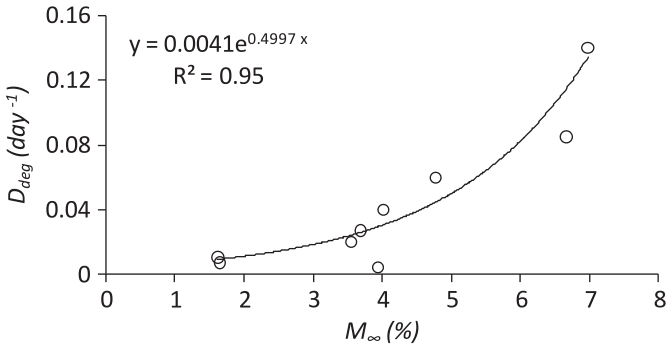

Fig. 11. Variation of the degradation coefficient of adhesive system 1 with the total fractional mass uptake, M_∞. Curve shows the least-squares exponential fit. Data points correspond to the nine T, RH conditions of Table 5.

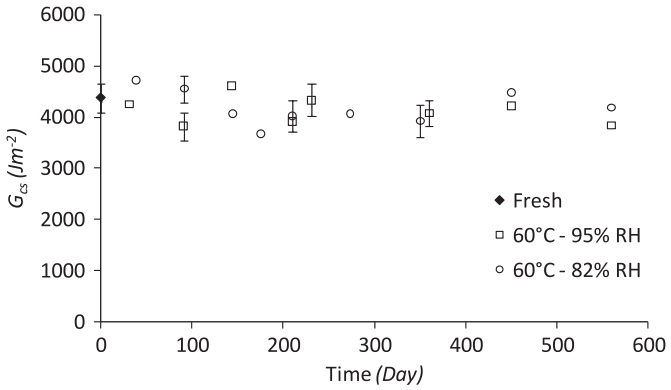

Fig. 12. Variation of G_{cs} tested at a phase angle of 27° with the exposure time at 60 °C-95% RH and 82% RH. Each data point without an error bar is an average of at least 20 measurements within one DCB specimen. Each data point with an error bar (± standard deviation) is an average value obtained from three different DCB specimens (at least 20 individual crack growth measurements from each).

scatter range (8%). Therefore, to a first approximation, the degradation condition (T and RH) affected only the rate of fracture strength degradation and not the final amount. It is noted that the time to reach the plateau value, ΔG_{cs}^{∞}, was generally much longer than the time to saturate the adhesive layer of the open-faced specimen and the difference between these two times was a strong function of RH at a given T. For example, at 60 °C, ΔG_{cs}^{∞} was reached after about 40 days (at 95% RH), 170 days (at 82% RH) and 360 days (at 43% RH), while the corresponding water saturation times were approximately 31, 66 and 104 days, respectively.

Fig. 9 shows that the degradation coefficient, D_{deg}, which reflects the rate of degradation (Eq. (2)) increased with an RH at any examined T, and was much more sensitive to an RH above approximately 80%. At a given RH, the degradation coefficient varied linearly with T between 20 and 60 °C (Fig. 10). It is reasonable to assume that the degradation rate was directly proportional to the water concentration in the primary adhesive layer. Since the time to water saturation was much less than the time to reach ΔG_{cs}^{∞}, the total fractional mass uptake (M_∞) was taken as a rough measure of the water content throughout the degradation; i.e. the lower concentration during the transient period of initial water uptake was ignored. As seen in Fig. 11, excluding the point (3.94, 0.004) corresponding to the 20 °C-95% RH condition, the degradation coefficient increased exponentially with M_∞ independent of T and RH. This is a useful result, because it simplifies the measurement and analysis of toughness degradation.

3.4.3. G_{cs} degradation in adhesive system 2

Fig. 12 shows that the variation of G_{cs} ($\psi = 27°$) of adhesive system 2 with an exposure time at 60 °C was entirely different from the pattern seen with adhesive system 1 (Figs. 6–8). No statistically significant (95% confidence) decrease was observed in the adhesive system 2 fracture toughness at either RH, even after 560 days of degradation. The G_{cs} value for the undegraded closed DCB specimens of adhesive system 2 (single-bonded DCB with a 400 μm bondline thickness) was 4380 Jm^{-2} with a standard deviation of 285 Jm^{-2}, and that of the degraded open-faced specimens, averaging all exposure times and conditions was 4160 Jm^{-2} with a standard deviation of 300 Jm^{-2}.

3.4.4. Degradation mechanisms

As discussed above, a key difference between the two adhesives was that adhesive 2 dried completely without retained water. Conversely, adhesive 1 retained a relatively large amount of water after drying, and consistent with the hypothesis that it was in the bound state (and therefore could not plasticize the matrix) the DMTA showed that T_g was unaffected by this retained water. As explained below, it is hypothesized that this bound water was responsible for the marked degradation in the fracture toughness of adhesive system 1.

The relatively high toughness of rubber-toughened epoxy adhesives arises from the energy dissipation associated with the deformation occurring at the crack tip, as it encounters rubber particles within the epoxy matrix. Such deformation includes cavitation at the particle/matrix interface and shear yielding in the adjacent matrix [39–41]. These toughening mechanisms are strongly affected by the adhesion between the rubber particles and matrix [42–44]. Therefore, a possible explanation for the rapid fracture toughness degradation of adhesive system 1 is that the retained water molecules disrupted chemical bonds between the rubber particles and the matrix by becoming bound at the

rubber–matrix interface. This hypothesis is supported by an earlier observation in Ref. [28] that mode I fracture tests of degraded joints of adhesive system 1 produced a G_{Ics} that decreased to a constant value in the range 510–790 Jm^{-2}, which was approximately equal to the mode I fracture strength reported for an untoughened DGEBA epoxy matrix (i.e. without rubber toughener particles); G_{Ics}=600 Jm^{-2} in [45] and 920 Jm^{-2} in [46]. In other words, the fracture resistance of the degraded adhesive 1 was similar to that of an untoughened epoxy matrix.

3.4.5. Degradation dependence on EI pathway

It has been proposed that an adhesive joint degradation at a given temperature is a function of the exposure index (*EI*), defined as the time integral of the water concentration in the joint [21]

$$EI = \int_{t_1}^{t_2} C(x,t)dt \tag{3}$$

This concept was motivated by the desire to combine the effects of time and water concentration, so that a single parameter could be used to quantify a given environmentally aging condition. For example, it was of interest to see whether a long exposure to a low RH environment would be equivalent to a shorter exposure to a high RH at a given temperature. Substituting $C(x,t)$ from Eq. (7) in Appendix into Eq. (3) and integrating over the absorption time gives the analytical expression for *EI* during the absorption as

$$\begin{aligned} EI_a = &\left\{ t + \frac{16h^2}{\pi^3 D_1} \sum_0^\infty \frac{(-1)^n}{(2n+1)^3} \left[\exp\left(\frac{-D_1(2n+1)^2\pi^2 t}{4h^2} \right) - 1 \right] \right. \\ &\left. \times \cos\left(\frac{(2n+1)\pi x}{2h} \right) \right\} C_{1\infty} + \varphi(t - t_d) \\ &\times \left\{ (t-t_d) + \frac{16h^2}{\pi^3 D_2} \sum_0^\infty \frac{(-1)^n}{(2n+1)^3} \left[\exp\left(\frac{-D_2(2n+1)^2\pi^2 (t-t_d)}{4h^2} \right) - 1 \right] \right. \\ &\left. \times \cos\left(\frac{(2n+1)\pi x}{2h} \right) \right\} C_{2\infty} \end{aligned} \tag{4}$$

where EI_a is the exposure index corresponding to the absorption process. Since the drying time of the open-faced specimens (7 days) was sometimes a significant fraction of the exposure time, the exposure index corresponding to the desorption process, EI_d was also considered. Substituting $C(x,t)$ from Eq. (10) in Appendix into Eq. (3) and integrating over the desorption time, t' gives the analytical solution for EI_d as

$$\begin{aligned} EI_d = C_r t' - &\left\{ \frac{16h^2}{\pi^3 D_d} \sum_0^\infty \frac{(-1)^n}{(2n+1)^3} \left[\exp\left(\frac{-D_d(2n+1)^2\pi^2 t'}{4h^2} \right) - 1 \right] \right. \\ &\left. \times \cos\left(\frac{(2n+1)\pi x}{2h} \right) \right\} (C_{1\infty} + C_{2\infty} - C) \end{aligned} \tag{5}$$

The total exposure index, EI_T from the time of first exposure to the hot-wet environment to the end of the drying period will then be

$$EI_T = EI_a + EI_d \tag{6}$$

At a given temperature, the diffusion coefficients D_1, D_2 and D_d in Eqs. (4) and (5) were independent of an RH [10], and for the open-faced specimens with a primary adhesive layer thickness of 0.4 mm, the variation of EI_a and EI_d through the thickness of the adhesive layer was negligible. EI_T was therefore taken as a function of absorption and desorption times and instantaneous water concentration calculated at the mid-plane half way through the thickness of the primary adhesive layer.

The *EI* concept is of use in quantifying environmental exposure only if the degradation is independent of the time-humidity path taken to reach a particular *EI*; i.e. the same amount of strength loss corresponding to a particular *EI* is observed after an exposure to different combinations of humidity and time, which give the same *EI*. The path independency of *EI* for adhesive system 1 was evaluated using combinations of three RH levels (95%, 82% and 43%) and different exposure times at 60 and 40 °C. Since there was no degradation in adhesive system 2 in the range of the exposure conditions and times studied, the path independency hypothesis could not be evaluated for this adhesive system.

Figs. 13 and 14 show the average G_{cs} values corresponding to particular EI_T values achieved by three different paths (95%, 82% and 43% RH) at 60 and 40 °C, respectively, for adhesive system 1. Figs. 15 and 16 show similar results at 50 °C (95% RH and 82% RH) and 20 ± °C (95% RH), respectively. EI_T values were calculated using Eqs. (4)–(6) and the experimental data given in Appendix (Table 6). A *t*-test showed that the difference between the G_{cs} values achieved from the different paths at temperatures of 40, 50 and 60 °C was statistically insignificant with 95% confidence for EI_T values greater than about 25×10^6 g/g s. For example, at 40 °C this value of EI_T corresponds to 64 days of exposure at 95% RH and 86 days at 82% RH. This finding is of

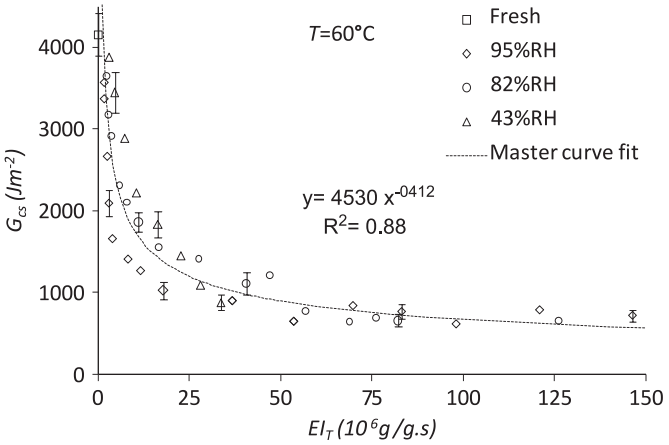

Fig. 13. Variation of G_{cs} with EI_T achieved by three different exposure paths (95%, 82% and 43% RH) at 60 °C. Each single data point is an average of at least 20 individual crack growth measurements within one DCB specimen. Each data point with an error bar is an average value obtained from three different DCB specimens (each with at least 20 individual crack growth measurements). Error bars show the standard deviation. Curve is least-squares power function fit to all data points.

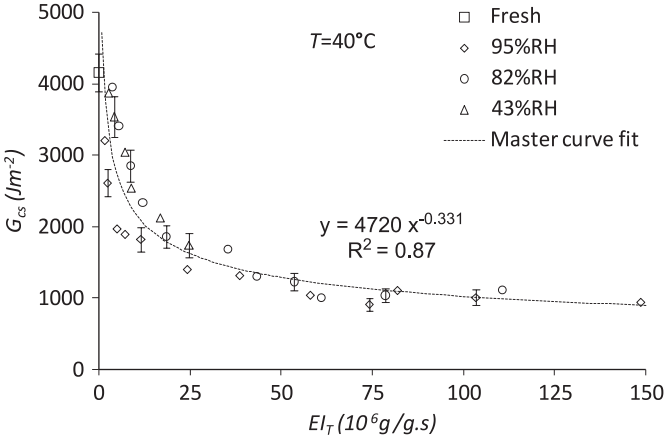

Fig. 14. Variation of G_{cs} with EI_T achieved by three different paths (95%, 82% and 43% RH) at 40 °C. Each single data point is an average of at least 20 individual crack growth measurements within one DCB specimen. Each data point with an error bar is an average value obtained from three different DCB specimens (each with at least 20 individual crack growth measurements). Error bars show the standard deviation. Curve is least-squares power function fit to all data points.

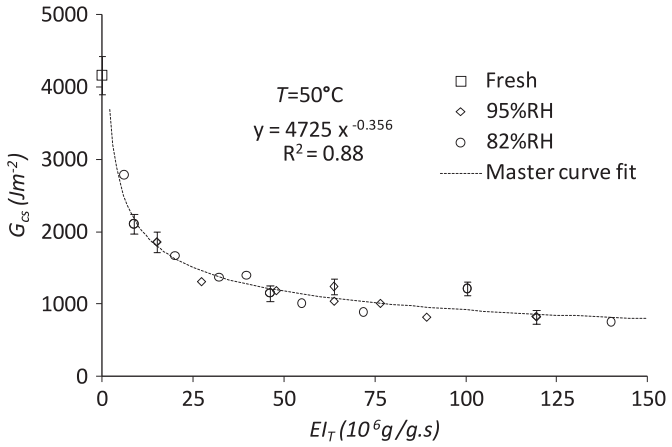

Fig. 15. Variation of G_{cs} with EI_T achieved by two different paths (95%, 82% RH) at 50 °C. Each single data point is an average of at least 20 individual crack growth measurements within one DCB specimen. Each data point with an error bar is an average value obtained from three different DCB specimens (each with at least 20 individual crack growth measurements). Error bars show the standard deviation. Curve is least-squares power function fit to all data points.

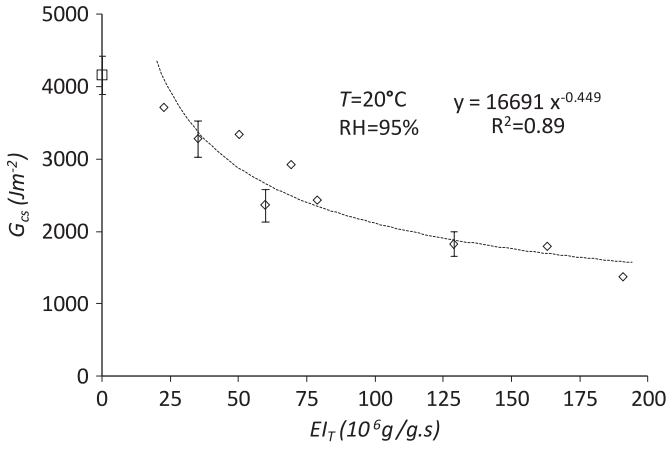

Fig. 16. Variation of G_{cs} with EI_T 95% RH and 20 °C condition. Each single data point is an average of at least 20 individual crack growth measurements within one DCB specimen. Each data point with an error bar is an average value obtained from three different DCB specimens (each with at least 20 individual crack growth measurements). Error bars show the standard deviation. Curve is least-squares power function fit to all data points.

practical interest, since it is usually intended to design adhesive joints for a long service life, where EI_T values would be large. For smaller EI_T, the degradation could not be said to be independent of the exposure history. For example, the 95% RH data points in both Figs. 13 and 14 lie below those for 82% and 43% RH. Because of the limited data available for smaller EI_T values at 50 °C, a strong conclusion could not be made about the degradation dependence on the exposure history at this temperature. Nevertheless, the master curves shown in Figs. 13–16 provide a useful envelope to estimate the amount of G_{cs} loss for any RH and exposure time at a given temperature. These relations can then be used to estimate the fracture strength of real joints that are exposed to varying condition (RH and temperature) during their service life by means of Eqs. (3)–(6).

Fig. 17 shows the best-fit curves of Figs. 13–16 for $EI_T > 25 \times 10^6$ g/g s, where the degradation was independent of the time–humidity pathway at a given temperature. It is seen that the degradation in the fracture strength increased with increasing temperature, tending to reach a quasi-steady level of residual strength for large values of EI_T in each case. The decrease in G_{cs} with an increasing temperature was quite uniform over a wide range of EI_T, and only at relatively small EI_T did the 20 °C curve diverge from being parallel to the others, indicating a greater sensitivity to temperature at lower values of an EI_T. To calculate EI_T values at a new condition, the required diffusion properties can be estimated using the predictive SDF model [10], and the corresponding G_{cs} can then be extrapolated from Fig. 17 with known values of EI_T and T. For example, Fig. 18 shows the variation of G_{cs} with T at selected EI_T values extracted from Fig. 17. A relatively good linear fit to $G_{cs}-T$

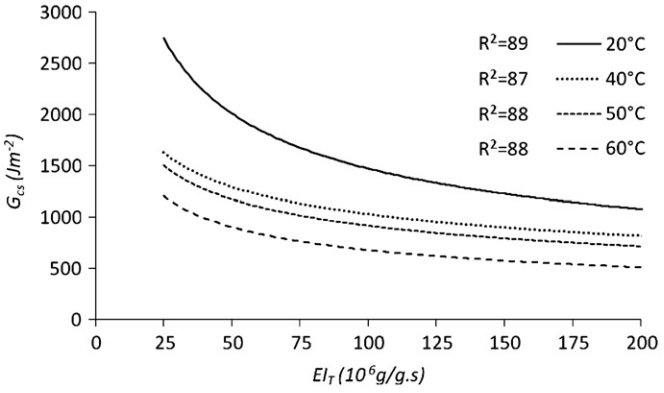

Fig. 17. Best-fit power law curves from Figs. 13 to 16.

Table 6
SDF model parameters of absorption and simple Fickian model parameters of desorption obtained by curve fitting the experimental gravimetric results at different T and RH for adhesives 1 and 2. Each data point is the average of measurements on three specimens. SD is the standard deviation [10].

T (°C)	RH (%)	$D_1 \pm$ SD (10^{-14} m^{2}s^{-1})	$D_2 \pm$ SD (10^{-14} m^{2}s^{-1})	$M_{1\infty} \pm$ SD (%)	$M_\infty \pm$ SD (%)	$t_d^{1/2}$ (s$^{1/2}$)	$D_d \pm$ SD (10^{-14} m^{2}s^{-1})	$M_r \pm$ SD (%)
Adhesive 1								
20	95	36 ± 6	3.9 ± 0.6	3.31 ± 0.05	3.94 ± 0.06	845	226 ± 21	1.07 ± 0.06
40	95	134 ± 17	3.8 ± 0.7	3.36 ± 0.09	4.78 ± 0.15	536	214 ± 22	1.40 ± 0.09
	82	142 ± 6	3.3 ± 0.4	2.71 ± 0.04	3.55 ± 0.06	524	202 ± 16	1.34 ± 0.04
	43	113 ± 11	0.0	1.65 ± 0.04	1.65 ± 0.04	∞	242 ± 19	0.86 ± 0.04
50	95	207 ± 9	4.5 ± 0.7	3.59 ± 0.08	6.67 ± 0.17	427	187 ± 14	1.63 ± 0.08
	82	222 ± 12	3.6 ± 0.4	2.71 ± 0.02	3.69 ± 0.04	416	212 ± 18	1.58 ± 0.05
60	95	314 ± 25	8.6 ± 0.9	3.73 ± 0.11	6.98 ± 0.18	329	172 ± 22	1.76 ± 0.11
	82	294 ± 28	4.9 ± 0.7	2.75 ± 0.05	4.02 ± 0.08	308	182 ± 26	1.98 ± 0.05
	43	271 ± 24	4.3 ± 0.8	1.38 ± 0.03	1.62 ± 0.04	924	186 ± 18	0.98 ± 0.03
Adhesive 2								
60	95	248 ± 29	8.1 ± 1.5	3.16 ± 0.09	4.78 ± 0.12	219	143 ± 13	0.16 ± 0.03
	82	208 ± 24	9.6 ± 1.3	2.38 ± 0.03	2.8 ± 0.04	273	151 ± 19	0.09 ± 0.02

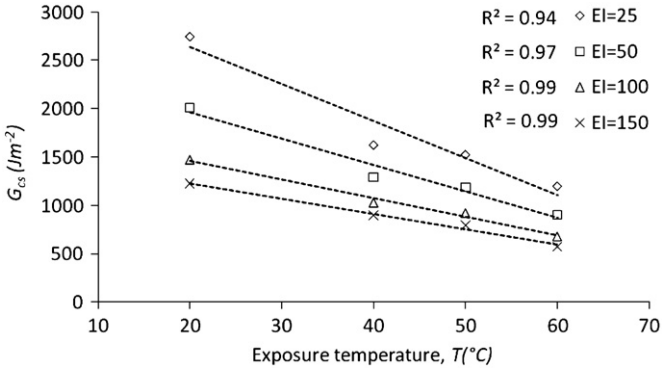

Fig. 18. G_{cs} variation with exposure temperature at different EI_T values extracted from Fig. 17. The lines show least-squares linear fits.

data at a given EI_T facilitates the calculation of G_{cs} at a new condition.

4. Conclusions

The differences between the absorption/desorption properties of two toughened epoxy adhesives were evaluated gravimetrically and by XPS and DMTA analyses. Both gravimetric and XPS results indicated that a significant amount of water was retained after drying in aged samples of adhesive 1, but a negligible amount was retained in adhesive 2. DMTA results showed that the retained water molecules in adhesive 1 were not free, but strongly bound with the adhesive constituents.

Mixed-mode fracture tests on degraded open-faced DCB specimens showed that the critical strain energy release rate, G_{cs} of adhesive system 1 decreased with an exposure time to reach a quasi-steady value that was similar to values reported for untoughened epoxy, while that of adhesive system 2 remained unchanged over a very long period. It was hypothesized that the differences in the degradation behavior and hygrothermal properties of the two adhesives were related to the presence of bound water molecules at the interface between the epoxy matrix and the rubber toughener in adhesive 1. Fickian-type degradation model (Eq. (2)) was proposed to characterize the fracture toughness loss in adhesive system 1, and fairly good agreement was observed between the model and the experimental results. The rate of degradation predicted by the model is controlled by the coefficient, D_{deg} which increased with the increasing temperature, RH and saturated water concentration.

The dependency of fracture toughness degradation on the humidity–time exposure history (pathway) was evaluated, using the concept of exposure index, *EI*. Even though the degradation could not be assumed to be fully independent of the exposure history, G_{cs}–*EI* curves provide a useful envelope to estimate the amount of G_{cs} loss at any exposure condition (RH and T) after relatively long exposure times.

Acknowledgments

The work was supported by General Motors Canada Ltd. and the Natural Sciences and the Engineering Research Council of Canada.

Appendix: Diffusion model

Based on the one-dimensional sequential dual Fickian (SDF) model presented in [10], the moisture concentration at any exposure time t and spatial coordinate x is determined by

$$C(x,t)=\left[1-\frac{4}{\pi}\sum_{n=0}^{\infty}\frac{(-1)^n}{2n+1}\exp\left(\frac{-D_1(2n+1)^2\pi^2 t}{4h^2}\right)\cos\frac{(2n+1)\pi x}{2h}\right]C_{1\infty}+\phi(t-t_d)\left[1-\frac{4}{\pi}\sum_{n=0}^{\infty}\frac{(-1)^n}{2n+1}\times\exp\left(\frac{-D_2(2n+1)^2\pi^2(t-t_d)}{4h^2}\right)\cos\frac{(2n+1)\pi x}{2h}\right]C_{2\infty} \quad (7)$$

where $C_{1\infty}$ and $C_{2\infty}$ are the saturated concentrations of the first and second diffusion mechanisms such that $C_{1\infty}+C_{2\infty}=C_{\infty}$, where C_{∞} is the total saturation concentration. D_1 and D_2 are the diffusion coefficients of the first and second moisture uptake mechanisms, respectively. t_d is the transition time between the first diffusion mechanism and the second, and $\Phi(t)$ is a Heaviside step function, which returns zero for negative values and one for positive values. By integrating Eq. (7) over the spatial variable, the fractional mass uptake, M_t for the SDF model at any time t is given by

$$M_t=\left[1-\frac{8}{\pi^2}\sum_{n=0}^{\infty}\frac{1}{(2n+1)^2}\exp\left(\frac{-D_1(2n+1)^2\pi^2 t}{4h^2}\right)\right]M_{1\infty}+\phi(t-t_d)\left[1-\frac{8}{\pi^2}\sum_{n=0}^{\infty}\frac{1}{(2n+1)^2}\right]\exp\left(\frac{-D_2(2n+1)^2\pi^2(t-t_d)}{4h^2}\right)\Bigg]M_{2\infty} \quad (8)$$

where $M_{1\infty}$ and $M_{2\infty}$ correspond to the first and second uptakes, respectively, and $M_{1\infty}+M_{2\infty}=M_{\infty}$. Assuming the uniform distribution of water concentration at saturation, $M_{1\infty}=C_{1\infty}$ and $M_{2\infty}=C_{1\infty}$. More details about the calculation of SDF model parameters can be found in [10]. The fractional mass uptake at any time t, M_t was determined experimentally using gravimetric measurements and its value is given by

$$M_t=\frac{W_t-W_i}{W_i}100\% \quad (9)$$

where W_i and W_t are the sample weights before any exposure and after exposure time of t, respectively.

Using Fick's law to model the desorption process, water concentration at desorption time t and spatial coordinate x are given by [10]

$$\frac{C(x,t)-C_r}{C_{\infty}-C_r}=\frac{4}{\pi}\sum_{n=0}^{\infty}\frac{(-1)^n}{2n+1}\exp\left(\frac{-D_d(2n+1)^2\pi^2 t'}{4h^2}\right)\cos\frac{(2n+1)\pi x}{2h} \quad (10)$$

where D_d and C_r are the diffusion coefficient of the desorption and the minimum retained water concentration, respectively. Integrating Eq. (10) over the spatial variable gives the fractional retained mass of water in the adhesive sample in percentage at desorption time t', M_t as

$$\frac{M_t-M_r}{M_{\infty}-M_r}=\frac{8}{\pi^2}\sum_{n=0}^{\infty}\frac{1}{(2n+1)^2}\exp\left(\frac{-D_d(2n+1)^2\pi^2 t'}{4h^2}\right) \quad (11)$$

where M_r is the minimum fractional retained water. The SDF absorption parameters (D_1, D_2, $M_{1\infty}$, $M_{2\infty}$, t_d) and the simple Fickian desorption parameters (D_d, M_r) for both adhesives are given in Table 6.

References

[1] Crank J. The mathematics of diffusion. Oxford: Oxford University Press; 1975.
[2] Wahab MA, Ashcroft IA, Crocombe AD, Shaw SJ. Diffusion of moisture in adhesively bonded joints. J Adhes 2001;77:43–80.

[3] LaPlante G, Ouriadov AV, Lee-Sullivan P, Balcom BJ. Anomalous moisture diffusion in an epoxy adhesive detected by magnetic resonance imaging. J Appl Polym Sci 2008;109:1350–9.
[4] Popineau S, Rondeau-Mouro C, Sulpice-Gaillet C, Shanahan MER. Free/bound water absorption in an epoxy adhesive. J Polym 2005;46:10733–40.
[5] Fernandez-Garcia M, Chiang MYM. Effect of hygrothermal aging history on sorption process, swelling, and glass transition temperature in a particle-filled epoxy-based adhesive. J Appl Polym Sci 2002;84:1581–91.
[6] Musto P, Ragosta G, Mascia L. Vibrational spectroscopy evidence for the dual nature of water sorbed into epoxy resins. Chem Mater 2000;12:1331–41.
[7] Roy S, Xu WX, Park SJ, Liechti KM. Anomalous moisture diffusion in viscoelastic polymers: modeling and testing. J Appl Mech 2000;67:391–6.
[8] Loh WK, Crocombe AD, Abdel Wahab MM, Ashcroft IA. Modeling anomalous moisture uptake, swelling and thermal characteristics of a rubber toughened epoxy adhesive. Int J Adhes Adhes 2005;25:1–12.
[9] Weir MD, Bastide C, Sung CSP. Characterization of interaction of water in epoxy by UV reflection spectroscopy. Macromolecules 2001;34:4923–6.
[10] Ameli A, Datla NV, Papini M, Spelt JK. Hygrothermal properties of highly toughened epoxy adhesives. J Adhes 2010;86:698–725.
[11] Mubashar A, Ashcroft IA, Critchlow GW, Crocombe AD. Moisture absorption–desorption effects in adhesive joints. Int J Adhes Adhes 2009;29:751–60.
[12] Lin YC. Investigation of the moisture-desorption characteristics of epoxy resin. J Polym Res 2006;13:369–74.
[13] Zhou J, Lucas JP. Hygrothermal effects of epoxy resin. Part I: the nature of water in epoxy. J Polym 1999;40:5505–12.
[14] Marsh LL, Lasky R, Seraphim DP, Springer GS. In: Springer GS, editor. Environmental effects on composite materials, 3. Westport: Technomic Publishing Co; 1988. p. 51.
[15] Moy P, Karasz FE. Epoxy–water interactions. Polym Eng Sci 1980;20:315–9.
[16] Carter HG, Kibler KG. Langmuir type model for anomalous moisture diffusion in composite resins. J Compos Mater 1978;12:118–31.
[17] Lin KF, Yeh RJ. Moisture absorption behavior of rubber-modified epoxy resins. J Appl Polym Sci 2002;86:3718–24.
[18] Zhou J, Lucas JP. Hygrothermal effects of epoxy resin. Part II: variations of glass transition temperature. Polymer 1999;40:5513–22.
[19] Xian G, Karbhari VM. DMTA based investigation of hygrothermal ageing of an epoxy system used in rehabilitation. J Appl Polym Sci 2007;104:1084–94.
[20] Loh WK, Crocombe AD, Abdel Wahab MM, Ashcroft IA. Environmental degradation of the interfacial fracture energy in an adhesively bonded joint. Eng Fract Mech 2002;69:2113–28.
[21] Wylde JW, Spelt JK. Measurement of adhesive joint fracture properties as a function of environmental degradation. Int J Adhes Adhes 1998;17:237–46.
[22] Liljedahl CDM, Crocombe AD, Abdel Wahab MM, Ashcroft IA. Modeling the environmental degradation of adhesively bonded aluminium and composite joints using a CZM approach. Int J Adhes Adhes 2007;27:505–18.
[23] Moidu A, Sinclair AN, Spelt JK. Adhesive joint durability assessed using open-faced peel specimens. J Adhes 1998;65:239–57.
[24] Greenspan L. Humidity fixed points of binary saturated aqueous solutions. J Res Natl Bur Stand—A: Phys Chem 1977;81A:89–96.
[25] ASHRAE Handbook:. Fundamentals. I-P ed.. American Society of Heating, Refrigerating and Air-Conditioning Engineers, Inc.; 2009. p. 1.1–1.20.
[26] ASTM D2651. Standard guide for metal surfaces for adhesive bonding. ASTM International West Conshohocken, PA; 2001.
[27] Ameli A, Papini M, Spelt JK. Fracture *R*-curve of a toughened epoxy adhesive as a function of aging. J. Mat. Sci. Eng. A. 2010;527:5105–14.
[28] Fernlund G, Spelt JK. Mixed-mode fracture characterization of adhesive joints. Comput Sci Technol 1994;50:441–9.
[29] Ameli A, Papini M, Schroeder JA, Spelt JK. Fracture *R*-curve characterization of toughened epoxy adhesives. Eng Fract Mech 2010;77:521–34.
[30] Fernlund G, Papini M, McCammond D, Spelt JK. Fracture load predictions for adhesive joints. Comput Sci Technol 1994;51:587–600.
[31] Xiao GZ, Delamar M, Shanahan MER. Irreversible interactions between water and DGEBA/DDA epoxy resin during hygrothermal aging. J Appl Polym Sci 1998;65:449–58.
[32] Montois P, Nassiet V, Petit JA, Adrian D. Viscosity effect on epoxy-diamine/metal interphases—Part II: Mechanical resistance and durability. Int J Adhes Adhes 2007;27:145–55.
[33] Ivanova KI, Pethrick RA, Affrossman S. Investigation of hydrothermal ageing of a filled rubber toughened epoxy resin using dynamic mechanical thermal analysis and dielectric spectroscopy. Polymer 2000;41:6787–96.
[34] Ivanova KI, Pethrick RA, Affrossman S. Hygrothermal aging of rubber-modified and mineral-filled dicyandiamide-cured DGEBA epoxy resin. II. dynamic mechanical thermal analysis. J Appl Polym Sci 2001;82:3477–85.
[35] De'Neve B, Shanahan MER. Water absorption by an epoxy resin and its effect on the mechanical properties and infra-red spectra. Polymer 1993;34:5099–105.
[36] Wang CH. On the fracture of constrained layers. Int J Fract 2006;93:227–46.
[37] Yan C, Mai Y, Ye L. Effect of bondline thickness on fracture behavior of adhesive joints. J Adhes 2001;75:27–44.
[38] Duan K, Hu X, Mai Y. Substrate constraint and adhesive thickness effects on fracture toughness of adhesive joints. J Adhes Sci Technol 2004;18:39–53.
[39] Banthia AK, Ratna D. Rubber toughened epoxy. Macromol Res 2004;12:11–21.
[40] Kinloch AJ. Structural adhesives: developments in resins and primers. London: Elsevier Applied Science; 1986. p. 127.
[41] Pearson RA, Yee AF. Toughening mechanisms in elastomer-modified epoxies, III: The effect of cross-link density. J Mater Sci 1989;24:2571–80.
[42] Collyer AA. Rubber toughened engineering plastics. London UK: Chapman and Hall; 1994. p. 30.
[43] Chen TK, Jan YH. Toughening mechanism for a rubber-toughened epoxy resin with rubber/matrix interfacial modification. J Mater Sci 1991;26. p. 5848–58.
[44] Chikhi N, Fellahi S, Bakar M. Modification of epoxy resin using reactive liquid (ATBN) rubber. Eur Polym J 2002;38:251–64.
[45] Thomas R, Yumei D, Yuelong H, Le Y, Moldenaers P, Weimin Y, et al. Miscibility, morphology, thermal, and mechanical properties of a DGEBA based epoxy resin toughened with a liquid rubber. J Polym 2008;49:278–94.
[46] Francis BV, Rao L, Jose S, Catherine BK, Ramaswamy R, Jose J, et al. Poly(ether ether ketone) with pendent methyl groups as a toughening agent for amine cured DGEBA epoxy resin. J Mater Sci 2006;41:5467–79.